ARMY RESEARCH LABORATORY

Modeling of Nano-Tungsten Sintering Data

by William S. de Rosset

ARL-CR-0665 **April 2011**

prepared by:

Dynamic Science, Inc.
8433 Black Canyon Hwy.
Phoenix, AZ 85021

under contract

W911QX09-0057

NOTICES

Disclaimers

The findings in this report are not to be construed as an official Department of the Army position unless so designated by other authorized documents.

Citation of manufacturer's or trade names does not constitute an official endorsement or approval of the use thereof.

Destroy this report when it is no longer needed. Do not return it to the originator.

Army Research Laboratory
Aberdeen Proving Ground, MD 21005-5069

ARL-CR-0665 **April 2011**

Modeling of Nano-Tungsten Sintering Data

William S. de Rosset
Weapons and Materials Research Directorate, ARL

prepared by:

Dynamic Science, Inc.
8433 Black Canyon Hwy.
Phoenix, AZ 85021

under contract

W911QX09-0057

REPORT DOCUMENTATION PAGE	Form Approved OMB No. 0704-0188

1. REPORT DATE *(DD-MM-YYYY)*	2. REPORT TYPE	3. DATES COVERED (From - To)
April 2011	Final	October 2010–February 2011

4. TITLE AND SUBTITLE
Modeling of Nano-Tungsten Sintering Data

5a. CONTRACT NUMBER
W911QX09-0057

5b. GRANT NUMBER

5c. PROGRAM ELEMENT NUMBER

6. AUTHOR(S)
William S. de Rosset

5d. PROJECT NUMBER
AH 84

5e. TASK NUMBER

5f. WORK UNIT NUMBER

7. PERFORMING ORGANIZATION NAME(S) AND ADDRESS(ES)
Dynamic Science, Inc.
8433 Black Canyon Hwy.
Phoenix, AZ 85021

8. PERFORMING ORGANIZATION REPORT NUMBER

9. SPONSORING/MONITORING AGENCY NAME(S) AND ADDRESS(ES)
U.S. Army Research Laboratory
ATTN: RDRL-WMM-F
Aberdeen Proving Ground, MD 21005-5069

10. SPONSOR/MONITOR'S ACRONYM(S)

11. SPONSOR/MONITOR'S REPORT NUMBER(S)
ARL-CR-0665

12. DISTRIBUTION/AVAILABILITY STATEMENT
Approved for public release; distribution is unlimited.

13. SUPPLEMENTARY NOTES

14. ABSTRACT

Small metal samples have been made from nano-crystalline tungsten powder by sintering with the goal of producing high density parts. The parameters associated with sintering runs have been examined to see if there is an empirical relationship between them and the final part density. A function that depends on the time the sample spends above a critical temperature has been formulated that represents one specific batch of tungsten powder. The function has been applied to other batches of powder with limited success. An attempt was made to use this function to arrive at the sintering parameters that would give a final density in excess of 95% that of theoretical density while retaining a nano-crystalline grain structure.

15. SUBJECT TERMS
sintering theory, nano-tungsten, grain size

16. SECURITY CLASSIFICATION OF:			17. LIMITATION OF ABSTRACT	18. NUMBER OF PAGES	19a. NAME OF RESPONSIBLE PERSON
a. REPORT	b. ABSTRACT	c. THIS PAGE			William S. de Rosset
Unclassified	Unclassified	Unclassified	UU	26	19b. TELEPHONE NUMBER (*Include area code*) 410-306-0816

Standard Form 298 (Rev. 8/98)
Prescribed by ANSI Std. Z39.18

Contents

List of Figures

List of Tables

Acknowledgments

The author is indebted to Eric Klier and Brady Butler for many helpful discussions on sintering theory and data interpretation. They were the ones responsible for generating the data found in this report. Thanks also go to James Catalano for providing a final polishing step that brought out the grain structure in the micrographs of the nano-crystalline tungsten and made the grain size determination more accurate. Finally, the author is grateful for the many micrographs taken by Bradley Klotz.

INTENTIONALLY LEFT BLANK.

1. Introduction

Sintering is a process which can be used to produce useful parts from metallic powder. It is accomplished by first compacting the powder and then heating the compacted form (greenware) until the powder is fused together. This process is currently being used in an attempt to produce tungsten penetrators from nano-crystalline tungsten powder. One approach that has been used at the U.S. Army Research Laboratory (ARL) is the Plasma Pressure Compaction method (*1*, *2*). This report deals with the conventional approach of simply heating the sample in a hydrogen atmosphere. The primary goal is to produce large parts that are fully dense but retain a nano-crystalline grain structure. It is surmised that if this can be achieved, the nano-tungsten penetrators will exhibit the same high-rate shear behavior during penetration as that of depleted uranium-3/4% titanium penetrators. This type of behavior produces superior penetration performance (*3*).

For the Depleted Uranium Replacement Program (DURP), the source of tungsten powder feed stock with a low (~1%) concentration of oxygen was the Chongyi Zhangyuan Tungsten Co., Ltd. Currently, this powder is wet-milled to break the agglomerated powder into finely-divided particles. The wet-milled slurry is then spray dried to remove the solvent. A compact of the powder is formed either by cold iso-static pressing or die pressing. Next, the compact is heated in vacuum to burn out contaminants. After heating the sample in a hydrogen atmosphere to remove the small amount of remaining oxygen, it is then heated to the sintering temperature at a given rate and held there for a given period of time. Clearly, the process of producing metal parts from powder requires many steps and processing variables.

The challenge to producing a fully-dense, nano-crystalline tungsten penetrator is that the sintering process leads to a larger grain size as the compacted powder is heated. It would be advantageous if the sintering process could be modeled and the parameters governing the process could be chosen to optimize the final density while at the same time keeping the grain size as small as possible. In section 2, it will be argued that the sintering process is relatively complicated, and no acceptable first-principle models of the entire process exist. Some progress has been made in establishing semi-empirical models, and the Master Sintering Curve (MSC) will be presented and discussed. In section 3, an alternative approach to the MSC is offered. This material-specific (MS) model takes a given powder and uses the sintering parameters of several different runs to fit a rationalized analytic function. In section 4, the advantages and limitations of the model are discussed. An attempt is made to use the MS model to guide the choice of sintering parameters to produce the greatest density while limiting grain growth. Section 5 summarizes the modeling effort.

2. Sintering Models

Sintering is such an important commercial process that it has been investigated by the scientific community for decades. Most of the fundamental understanding of the process has come through the study of two spherical particles that are placed in contact. Three stages of sintering have been identified, with the importance of surface diffusion, grain boundary diffusion, and volume diffusion being different in each of the stages in chapter 3 of German (*4*). Some progress in modeling the sintering process has been made with computer models that take into account more than one form of mass transport. However, most models do not consider the complexity of the sintering process. For instance, powders are not made up of single-size, single-component spherical particles as assumed by many models. There may be materials added in small quantities to assist in the sintering process that are not accounted for. The same can be said of small amounts of contaminants. The sintering process is often carried out in a reducing or oxidizing atmosphere, generally neglected by most models. Many models assume a rapid heating rate that is not possible to impose on the sample without thermal shock and cracking in chapter 1 of German (*4*).

Alternatively, one can adopt an empirical or semi-empirical approach to modeling the sintering process. One such model is the MSC (*5*). This model relates the shrinkage rate during sintering to a function of surface energy γ, absolute temperature T, mean grain diameter G, atomic volume Ω, Boltzmann's constant k, the width of a grain boundary δ, coefficients for grain-boundary and volume diffusion (D_b and D_V, respectively), and two scaling parameters (Γ_b and Γ_V). The expression can be simplified by assuming only one bulk transport mechanism, either $D_o = D_V$ or $D_o = \delta D_b$. In this case, the scaling parameters, determined experimentally, collapse into one value, Γ. Then,

$$\frac{1}{3\rho}\frac{d\rho}{dt} = \frac{\gamma\Omega\Gamma(\rho)D_o}{kT(G(\rho))^n}\exp\left(-\frac{Q}{RT}\right), \qquad (1)$$

where ρ is the density, n = 3 or 4 depending on the transport mechanism, Q is the apparent activation energy, and R is the gas constant. After further manipulation, equation 1 can be integrated by separating variables. (This mathematical operation is somewhat questionable, since it assumes that G and Γ are independent of time. However, both these parameters depend on density, which is a function of time as shown in equation 1.) The contention then is that an MSC can be generated by conducting a series of experiments that measure the dimensional changes at different heating rates. This information then gives the density as a function of the sintering parameters.

Su and Johnson (*5*) point out the limitations of the MSC. First, it should only be applied to powder compacts made from the same powder and same green-body processing. Second, their assumption that Γ depends only on density has not been generally shown to be true. Third, it

may be that more than one diffusion mechanism is operating during the sintering process. However, the authors state that deviations from a single mechanism can be readily observed.

Butler et al. (*6*) have successfully applied the MSC approach to the sintering of nano-crystalline tungsten. Dilatometer measurements were made at three different heating rates (3 °C/min, 5 °C/min, and 25 °C/min) for each of three materials with different thermal stabilities. These data were then used to generate the MSCs. These curves give the material density as a function of the sintering parameters from the initial sintering stage (~40% theoretical density) to the final stage (~90% theoretical density).

3. MS Sintering Model

An alternative approach to modeling was sought that would try to capture the effect of the important sintering parameters in an uncomplicated manner. Equation 2 is an example of such a simple model:

$$\Psi = t \exp(- Q/kT), \tag{2}$$

where Ψ is the degree of sintering, t is the time, Q is an activation energy, k is Boltzmann's constant, and T is the absolute temperature in chapter 4 of German (*4*) . It is intuitive that a longer sintering time can lead to a greater material density (i.e., degree of sintering). However, there is certainly a limit to the process. Thus, some form of time limit would be needed to apply equation 2 to a real sintering process. Also, Ψ would have to be defined in terms of measurable parameters.

The first step taken in developing a simple model was to examine a representative sintering data set. The intention was to see if some analytical form could be used to fit the data. The form would be suggested by the important trends in the data. The data set chosen was all the sintering runs taken from mill run Wn-MT-34. (Here, Wn stands for nano-tungsten, MT stands for milling trial, and 34 identifies which trial.) This was the first mill run that resulted consistently in sintered samples with small (~200 nm) grain sizes. In addition, many sintering runs were made from the mill run with a wide variation in sintering parameters so that a better sense of what was important could be obtained.

Results from the sintering runs made with the mill run Wn-MT-34 powder are shown in table 1. The first column identifies the sintering run, and the second column shows the hydrogen reduction step. The third column shows the sintering temperature and the fourth column the heating and cooling rates. Typically, the sample was cooled at twice the heating rate. The holding time, HT, at the sintering temperature is shown in the fifth column. The percent theoretical density was determined by weighing the sample in air and water and using 19.3 g/cm^3 as the theoretical density. The grain size is shown in the last column. The appendix explains

how this value was determined. In the last entry in the table, the heating cycle was not completed, so the grain size measurement was not taken. All sintering data were taken from the original log entries. Three of the entries in table 1 are marked with an asterisk. These are exceptional runs that resulted in a high density (>95% theoretical density) and a small grain size (~150 nm or less).

Table 1. Sintering run data for Wn-MT-34.

Sintering Identification	Hydrogen Reduction	Sintering Temperature °C	Heating/Cooling Rate °C/min	Sintering Time	Theoretical Density (%)	Grain Size (nm)
Wn-SST-49-p1*	3 h at 700 °C	1400	5/10	1 s	95.15	143
Wn-SST-50-p2	3 h at 700 °C	1300	5/10	1 s	90.2	132
Wn-SST-50-p3	3 h at 700 °C	1300	5/10	1 s	89.12	128
Wn-SST-51-p4*	3 h at 800 °C	1400	5/10	1 s	95.77	147
Wn-SST-51-p5*	3 h at 800 °C	1400	5/10	1 s	96.24	128
Wn-SST-52-p8-1	3 h at 700 °C	1400	25/50	1 s	89.73	124
Wn-SST-52-p8-2	3 h at 700 °C	1400	25/50	1 s	88.19	108
Wn-SST-53-p8-3	3 h at 700 °C	1400	25/50	30 min	91.29	838
Wn-SST-54-p8-4	3 h at 700 °C	1300	25/50	1 s	85.88	111
Wn-SST-55-p7-1	3 h at 700 °C	1400	25/50	4 h	95.90	189
Wn-SST-56-p7-2	3 h at 700 °C	1300	25/50	4 h	95.49	300
Wn-SST-57-p6	2.5 h at 700 °C	1400	7.3 to 1100 °C 3.7 to 1400 °C 7.3 to 500 °C	30 min	96.21	194
Wn-SST-58-p7-3	3 h at 700 °C	1200	25/50	30 min	84.80	112
Wn-SST-59-p7-4	3 h at 700 °C	1500	25/50	30 min	96.68	159
Wn-SST-60-p7-5	3 h at 700 °C	1500	25/50	1 s	95.17	162
Wn-SST-61-p8-5	3 h at 700 °C	1300	25/50	30 min	87.83	143
Wn-SST-64-p9-1	3 h at 700 °C	1500	25/50	4 h	95.16	301
Wn-SST-65-p9-2	3 h at 700 °C	1600	25/50	1 s	94.74	150
Wn-SST-66-p10	3 h at 700 °C	1600?	N/A	30 min	91.69	—

These data were examined to extract a functional relationship between the final material densities to the sintering parameters, if possible. The two major requirements on the relation were that it should incorporate all the major controllable sintering parameters (time, temperature, and heating/cooling rates) and that it have a plausible basis. The relationship should also conform to physical reality in that the final density should not exceed the theoretical density. A desirable feature of the function is that it contains as few fitting parameters as possible.

All the sintering runs for Wn-MT-34 were conducted at a maximum sintering temperature T equal to or greater than 1200 °C. It was reasoned that it is important to have the sintering temperature above a certain value for a reasonable length of time in order to achieve the highest final density. Several functions were considered that fit the data to some extent and met most or all of the imposed requirements. The one chosen met all the requirements and was the simplest in form. Let the percent theoretical density be ρ/ρ_o and t the time the sample is above a critical

temperature T_o. A function that describes the data over the observed range of parameters is given by

$$\rho/\rho_o = 1 - 1/(t^{(T - T_o)/T_o}). \quad (3)$$

The percent theoretical density approaches 1.0 as the values of t and $(T-T_o)/T_o$ become large. Here, t is measured in minutes. Note that the time held at the maximum sintering temperature (*HT*) as well as both the heating and cooling rates are needed to determine t. Realistic heating and cooling rates, as well as values of T much larger than T_o, insure that t is large enough to avoid negative values of ρ/ρ_o.

Data for a sintering temperature of 1400 °C is shown in figure 1, along with the fitted function taken from equation 3. A best fit to the data was obtained by letting T_o be 860 °C. A similar plot is shown in figure 2 for the 1300 °C sintering temperature.

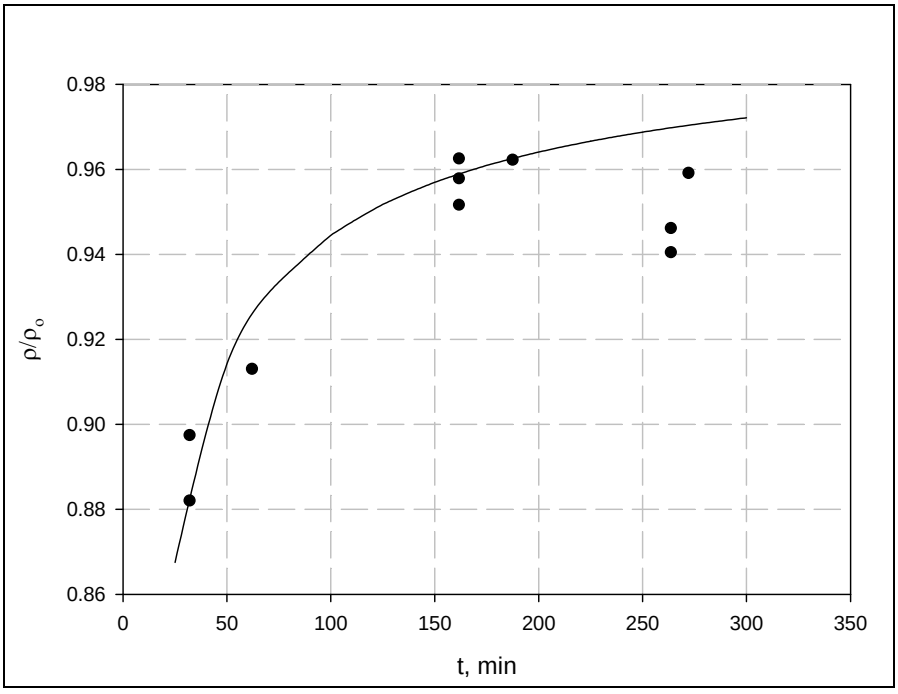

Figure 1. Comparison of data and functional fit for T = 1400 °C and T_o = 860 °C.

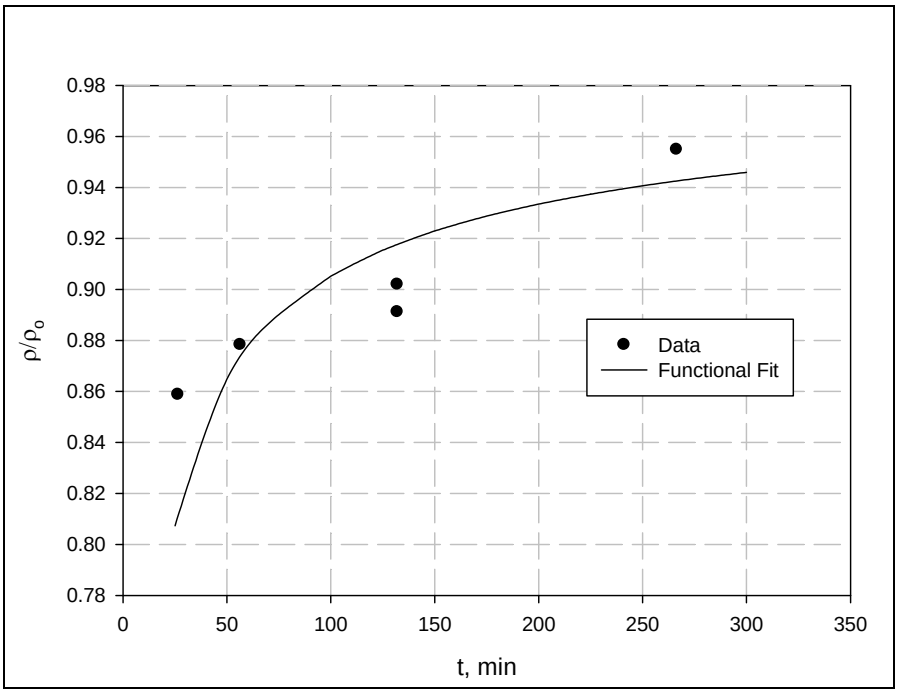

Figure 2. Comparison of data and functional fit for T = 1300 °C and T_o = 860 °C.

One sintering run was conducted at 1200 °C. The model predicts the sintered part to have a density 79% that of theoretical density, whereas the actual measured value was 84.8%. This disagreement may be due to the steepness of the curve for $0 < t < 50$.

4. Discussion

The fitting function in equation 3 is restricted to one mill run, so its usefulness in predicting the results for sintering runs from other mill runs is open to question. However, the general trend of other data sets might be represented by the function. To examine this possibility, another mill run was selected that had a large number of sintering trials, Wn-MT-35. Each of the sintering runs with this milling batch was done at a fast heating rate, interpreted as 25 °C/min, except for Wn-SST-68, which used program 5 (heat at 50 h to 700 °C, hydrogen reduction at 700 °C for 3 h, heat to 1400 °C at 220 °C/h, hold for 3 h, cool at 440 h to 500 °C, cool to room temperature at 50 °C/h). The runs had various hold times at the sintering temperature. Table 2 gives the relevant parameters for these sintering runs. None of these runs had grain sizes below 150 nm. However, the theoretical densities were all equal to or above 93% with only one exception.

The predicted densities are plotted versus the model in figure 3 for T = 1400 °C and T_o = 860 °C. The data appear to fall near the predicted curve, except for 67-FC6. This run produced a substantially lower density sample than the identically-processed 67-FC11. One possible explanation for this difference is that a large crack was observed in sample 67-FC11. It is

surmised that this crack occurred during the initial hydrogen reduction phase of the process, leading to a higher diffusion of hydrogen into the interior of the sample. This was a large sample (22 g as opposed to the usual 3–5 g), and the heating rate was high, so differences from this crack would magnify the degree of reduction and hence differences in final densities (*7*). The agreement between the predicted and observed values of the density achieved for sintering runs using milling run Wn-MT-35 is encouraging, especially considering that the fitting parameter T_o was not changed.

Table 2. Sintering parameters for mill run Wn-MT-35.

Sintering Identification	T (°C)	HT (min)	Measured ρ/ρ_o	Predicted ρ/ρ_o	Grain Size (nm)
61-3p1-1	1300	30	0.9470	0.877	171
62-3p2	1400	30	0.9707	0.950	182
63-3p1-2	1400	30	0.9083	0.928	197
64-3p1-3	1500	240	0.9564	0.986	275
65-3p3-1	1600	0	0.9624	0.963	212
67-FC6	1400	240	0.9081	0.972	194
67-FC11	1400	240	0.9676	0.972	215
68-FCp9	1400	30	0.9767	0.970	161
73-3p3-2	1400	120	0.9679	0.959	181

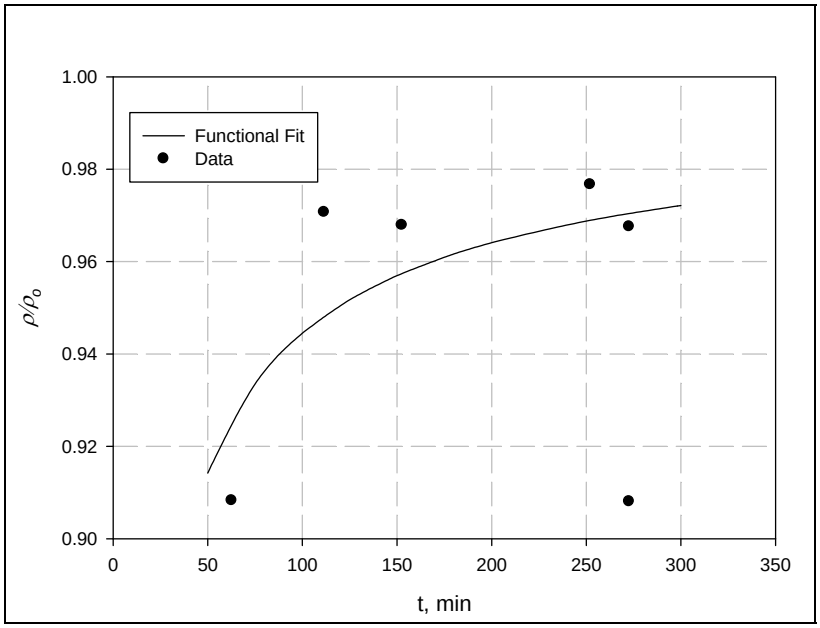

Figure 3. Comparison of data and model for T = 1400 °C, T_o = 860 °C, Wn-MT-35.

Sintering trials from a third mill run were examined, given the apparent agreement between the model and mill runs Wn-MT-34 and -35. The run chosen was labeled N6. Its source was Netzsch, Inc., who used the ZX powder as the starting point. However, processing parameters used to produce the powder are not known. A plot of the data and model predictions is shown in figure 4. Again, 860 °C was used as T_o. The fit is very poor, and it may be that the parameter t is inappropriate for this mill run.

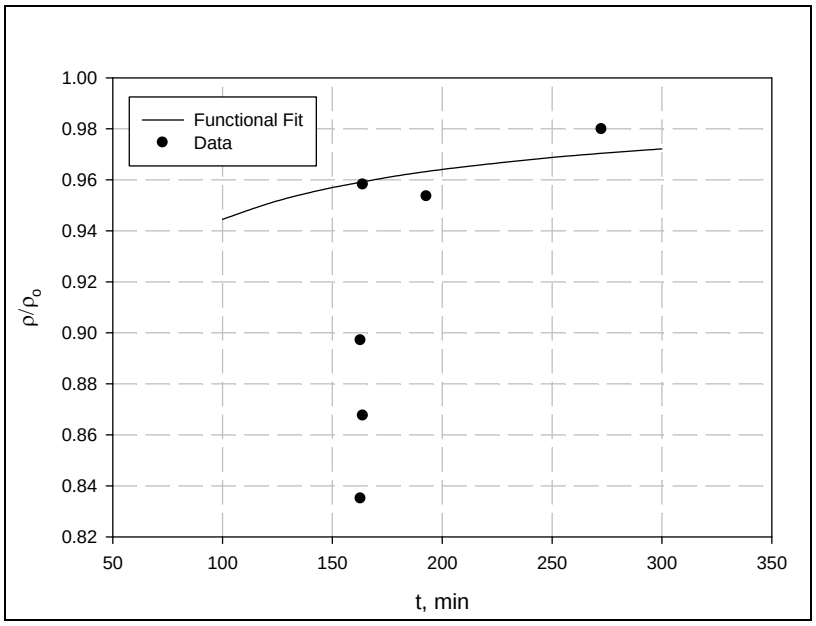

Figure 4. Comparison of data and model for T = 1400 °C, T_o = 860 °C, mill run N6.

Subsequent mill runs were carried out with the intention of scaling the entire process up to make larger specimens. The model was used to predict the final densities resulting from sintering runs using those mill run outputs. Little success was achieved, however. This could have been due to change in mill process parameters or the fact that the specimens were larger in mass.

The model can be used to suggest the combination of sintering parameters that gives the highest density while retaining a small grain size. We expect that as the sintering time increases, grain growth will occur. Therefore, we use the model to predict the minimum value of t necessary to achieve 95% theoretical density.

We first start out by assuming that we use a cooling rate is twice the heating rate, HR (°C/min). We also assume a 30 min hold at T. Given a value of T and T_o = 860 °C, we can calculate the value of t. This value can then be used in equation 3 to find the per-cent theoretical density of the sample. These calculations were carried out with the results shown in table 3. (Note that the highest value of HR is outside the sintering parameter range actually used in this study.)

From an examination of the values of t, the combination of T = 1500 °C and HR = 30 °C/min gives the lowest value of t to reach 95% of theoretical density (t = 62 min).

Table 3. Predicted fraction of fully dense W.

HR	T	1300	1400	1500	1600
5	—	0.929	0.965	0.983	0.992
10	—	0.906	0.950	0.974	0.986
15	—	0.893	0.940	0.967	0.982
20	—	0.883	0.933	0.962	0.979
25	—	0.877	0.928	0.958	0.976
30	—	0.871	0.923	0.955	0.974

Table 1 does not show any run at T = 1500 °C that was exceptional. However, there were two runs (WN-SST-59-p7-4 and WN-SST-60-p7-5) that achieved densities over 95% theoretical density but had slightly larger grain sizes (159 and 162 nm, respectively). Given the uncertainty in the grain size measurement, they also might be considered exceptional. Three runs conducted at 1400 °C were exceptional. According to the model, the fastest heating rate that produces a sample with 95% theoretical density for a sintering temperature of 1400 °C is 10 °C/min. The time t in this case is 112 min, or almost twice that for the 1500 °C sintering temperature run. Of course, this result would change if the sample were held at the sintering temperature for times different from the 30 min used in this example.

Most of the sintering runs were conducted at a temperature of 1400 °C. Perhaps if more runs had been carried out at 1500 °C there would have been more exceptional runs at this sintering temperature. However, the model does not support the supposition that just minimizing the time above T_o will result in a small grain size. The maximum sintering temperature must be considered also.

While no definitive statement can be made concerning the maximum sintering temperature, it can be brought into the analysis in the following way. First, we select a desired value of ρ/ρ_o. For our example, 0.95 is chosen. This is an arbitrary choice, and the analysis can be carried out for other values. In this case,

$$0.95 = 1 - 1/(t^{(T - T_o)/T_o}), \tag{4}$$

from equation 3. Further manipulation yields

$$((T - T_o)/T_o) \ln(t) = \ln 20. \tag{5}$$

Noting that

$$t = 1.5(T - T_o)/HR + HT. \tag{6}$$

where HT is the hold time at the maximum sintering temperature, values of t and T can be generated for given values of HT and HR. Here, we have assumed a cooling rate that is twice the

heating rate. We arbitrarily set the value of *HT* to 30 min and examine the relationship among *t*, *T*, and *HR*. These results are shown in table 4.

Table 4. Values of *t* and *T* from model predictions.

HR (°C/min)	t (min)	T (°C)
20	74.8	1457
22.5	70.4	1466
25	66.8	1473
27.5	63.8	1480
30	61.3	1486
32.5	59.1	1491
35	57.3	1496

In addition to minimizing *t*, it is reasonable to assume that small grain growth will occur for a minimum value of *T*. However, according to the model and our assumptions concerning the other parameters, *t* and *T* cannot be minimized simultaneously.

Other considerations may dictate the choice of *HR*. For instance, large samples may need a relatively low value of *HR* so that the entire sample heats and cools at about the same rate. Low values of *HR* can lead to high values of *t*. In this case, the holding time can be reduced to compensate for this large value.

5. Summary

A brief review of sintering theory indicated that no first-principles theory was available to model this complicated process. Instead, an empirical approach was used to organize sintering data for a specific mill run. One functional form that appeared to fit the data for mill run Wn-MT-34 was based on the time *t* the powder sample was held above a critical temperature, T_o, used as a single-fitting parameter. This mill run was chosen because there were many sintering runs made from the same batch of powder. The same function and fitting parameter were used to fit the data from another mill run (Wn-MT-35) with reasonable success. However, further attempts to use the same function and fitting parameter on other mill runs did not have as good a result. This may have been due to a difference in the starting powder or the fact that many of the sintered samples examined were much larger than those in mill runs Wn-MT-34 and -35. Even so, it is clear that if some attention is paid to keeping the powder processing parameters the same, as well as the sample masses, the possibility exists that the final density can be predicted using values of the controllable sintering parameters, based on a model for one mill run.

The functional relationship between the sintering parameters and the final density was used in an attempt to predict optimum sintering parameters. It was assumed that a very small grain size would be achieved with the minimum time necessary to achieve 95% of theoretical density. The model predicted that a minimum time *t* of 62 min would be needed to obtain 95% of the theoretical density for *T* = 1500 °C and a fast heating rate. While this value of *T* produced two cases (Wn-SST-59-p7-4 and Wn-SST-60-p7-5) where the grain sizes were reasonable (159 and 162 μ, respectively), there were other instances where smaller grain sizes were achieved with a lower sintering temperature. By restricting the range of parameters and setting the desired final density at a fixed percentage of theoretical density, the relationship among *t*, *T*, and *HR* can be found. The results indicated that the value of *t* and *T* could not be minimized simultaneously.

6. References

1. Klotz, B. R.; Kellogg, F. R.; Klier, E. M.; Dowding, R. J.; Kyu, C. C. *Characterization, Processing, and Consolidation of Nanoscale Tungsten Powder*; ARL-TR-5045; U.S. Army Research Laboratory: Aberdeen Proving Ground, MD, 2009.
2. Klotz, B. R.; Kellogg, F. R.; Cho, C. C. *Characterization and Consolidation of Tungsten Nanopowders Produced by Salt-Assisted Combustion Synthesis*; ARL-TR-5311; U.S. Army Research Laboratory: Aberdeen Proving Ground, MD, 2010.
3. Magness, L. S. High Strain Rate Deformation Behaviors of Kinetic Energy Penetrator Materials during Ballistic Impact. *Mechanics of Materials* **1994**, *17*, 147–154.
4. German, R. M. *Sintering Theory and Practice*; John Wiley and Sons: New York, 1996.
5. Su, Hunghai; Johnson, D. L. Master Sintering Curve: A Practical Approach to Sintering. *J. Am Cer Soc* **1996**, *79* (12), 3211–3217.
6. Butler, B.; Klier, E.; Kelley, M.; Gallagher, M.; Maupin, H. *Thermal Stability of Milled Nanocrystalline Tungsten Powders*; ARL technical report to be published.
7. Butler, B. Private communication, 2011.
8. ASTM E 112-96. *Annu. Book ASTM Stand*. Re-approved 2004.

Appendix. Grain Size Measurement

Samples were prepared for viewing on the scanning electron microscope by polishing them with successively finer grit papers. This continues until the surface is smooth enough to be polished with 1-micron (or less) powder. Micrographs were then taken of these samples. The grain boundary intersection count was used to determine an approximate grain size. This is done by overlaying a grid on the micrograph and counting the number of times the grid lines intersect a grain boundary. Dividing the length of the grid by the number of intersection points gives the result. (Note: this is really the mean lineal intercept length as defined by American Society for Testing and Materials (ASTM) (*8*). Since there is no direct mathematical relationship between the mean lineal intercept length and the grain size number G, we simply use it as an average grain size.)

This method works well when the grain boundaries are easily distinguishable. However, the polishing resulted in a somewhat blurry picture of the nano-crystalline microstructure. Fortunately, a final polishing step was found that brought out the microstructure of the already-polished samples. It consisted of using 0.05-micron colloidal silica in conjunction with chromic trioxide (an attack etch). An example of a micrograph of a sample after this final step was applied is shown in figure A-1.

The length of this grid is 14 μ, as determined from the scale marking on the photomicrograph. The magnification of this particular micrograph was 50,000×. However, for samples with larger grain sizes, a smaller magnification was used. This was done to meet the general requirement to have at least 50 intersections on the grid. In this case, the grid size changes also.

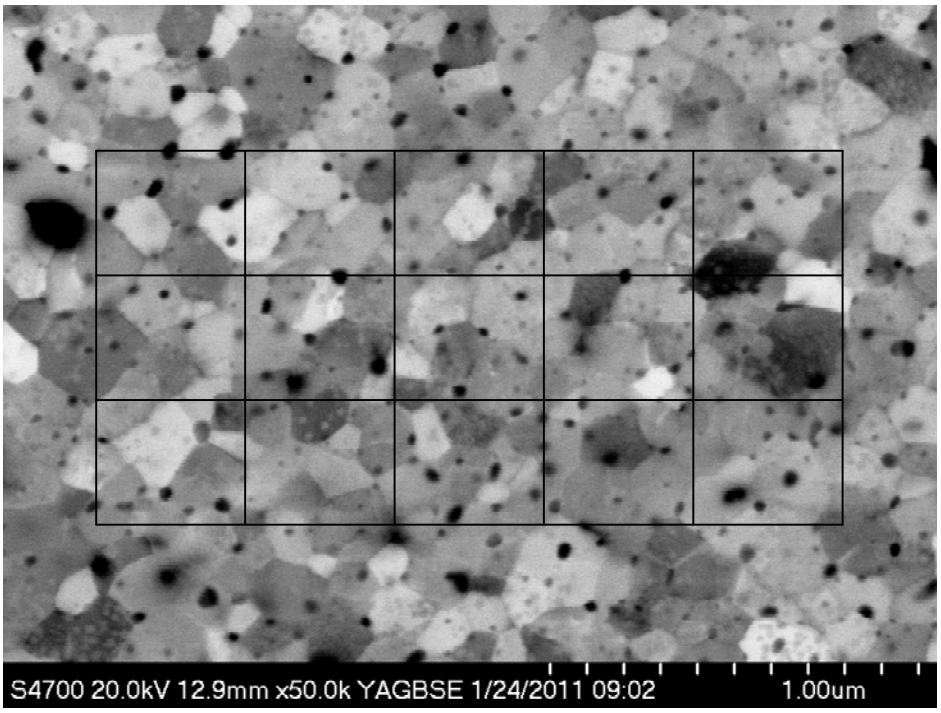

Figure-A 1. Micrograph of sample SST-51-P4.

List of Symbols, Abbreviations, and Acronyms

ARL	U.S. Army Research Laboratory
ASTM	American Society for Testing and Materials
DURP	Depleted Uranium Replacement Program
MS	material-specific
MSC	Master Sintering Curve
MT	milling trial
SST	Self-Sintering Trial
Wn	nano-tungsten

NO. OF COPIES	ORGANIZATION
1 (PDF only)	DEFENSE TECHNICAL INFORMATION CTR DTIC OCA 8725 JOHN J KINGMAN RD STE 0944 FORT BELVOIR VA 22060-6218
1	DIRECTOR US ARMY RESEARCH LAB IMNE ALC HRR 2800 POWDER MILL RD ADELPHI MD 20783-1197
1	DIRECTOR US ARMY RESEARCH LAB RDRL CIM L 2800 POWDER MILL RD ADELPHI MD 20783-1197
1	DIRECTOR US ARMY RESEARCH LAB RDRL CIM P 2800 POWDER MILL RD ADELPHI MD 20783-1197
1	DIRECTOR US ARMY RESEARCH LAB RDRL D 2800 POWDER MILL RD ADELPHI MD 20783-1197
	ABERDEEN PROVING GROUND
1	DIR USARL RDRL CIM G (BLDG 4600)

NO. OF COPIES ORGANIZATION

1 COMMANDER
US ARMY MATERIEL CMD
AMXMI INT
9301 CHAPEK RD
FORT BELVOIR VA 22060-5527

2 PM ARMS
SFAE AMO MAS MC
BLDG 354
PICATINNY ARSENAL NJ
07806-5000

1 US ARMY ARDEC
AMSRD AAR AEM L
D VO
BLDG 65 SOUTH
PICATINNY ARSENAL NJ
07806-5000

1 US ARMY ARDEC
AMSRD AAR AEM
S MUSALLI
BLDG 65 SOUTH
PICATINNY ARSENAL NJ
07806-5000

1 US ARMY ARDEC
AMSRD AAR EI
R CARR
BLDG 65N
PICATINNY ARSENAL NJ
07806-5000

1 PM ARMS
SFAE AMO MAS
BLDG 354
PICATINNY ARSENAL NJ
07806-5000

1 US ARMY RDECOM-TARDEC
SURVIVABILITY LEAD MRAP
JPO PEO GROUND COMBAT SYS
AMSTA TR S
D TEMPLETON
6501 E 11 MILE RD MS 263
WARREN MI 48397-5000

NO. OF COPIES ORGANIZATION

4 BENET WEAPONS LABS
AMSTA AR CCB
E KATHE
AMSTA AR CCB R
S SOPOK
R DILLON
AMSTA AR CB R
E HYLAND
WATERVLIET ARSENAL
BLDG 115
1 BUFFINGTON ST
WATERVLIET NY 12189-4050

3 BENET WEAPONS LABS
A CRAYON
M MILLER
F CAMPO
WATERVLIET ARSENAL
BLDG 115
1 BUFFINGTON ST
WATERVLIET NY 12189-4050

7 DIRECTOR
US ARMY NGIC
D LEITER MS 404
M HOLTUS MS 301
M WOLFE MS 307
S MINGLEDORF MS 504
J GASTON MS 301
W GSTATTENBAUER MS 304
J CRIDER MS 306
2055 BOULDERS RD
CHARLOTTESVILLE VA
22911-8318

3 US ARMY RSRCH OFC
RDRL ROE M
J PRATER
D STEPP
RDRL ROP C
D KISEROW
PO BOX 12211
RESEARCH TRIANGLE PARK NC
27709-2211

1 DARPA
S WAX
3701 N FAIRFAX DR
ARLINGTON VA 22203-1714

NO. OF COPIES ORGANIZATION

ABERDEEN PROVING GROUND

40 DIR USARL
RDRL LOA F
M ADAMSON
RDRL WM
P PLOSTINS
J MCCAULEY
B FORCH
RDRL WML
J NEWILL
M ZOLTOSKI
RDRL SET
T KOGLER
RDRL WML B
R PESCE-RODRIGUEZ
B RICE
R LIEB
RDRL WML D
P CONROY
RDRL WML G
W DRYSDALE
RDRL WMM
R DOWDING
RDRL WMM A
R EMERSON
RDRL WMM B
T BOGETTI
B CHEESEMAN
RDRL WMM D
E CHIN
D GRANVILLE
W ROY
RDRL WMM E
J SWAB
J LASALVIA
RDRL WMM F
R CARTER
W DE ROSSET
L KECSKES
J MONTGOMERY
D SNOHA
H MAUPIN
B BUTLER
E KLIER
B KLOTZ
RDRL WML G
M MINNICINO
M BERMAN
A ABRAHAMIAN
RDRL WMP
P BAKER
S SCHOENFELD
RDRL WMP B
C HOPPEL
RDRL WMP C
T BJERKE
RDRL WMP D
J RUNYEON
T HAVEL
RDRL WMP E
M BURKINS